PHYSICAL REVIEW C VOLUME 4, NUMBER 2 AUGUST 1971

Measurement and Analysis of Ground-State Band Transitions and $2^{+\prime}$ States in ^{78,80,82,84}Kr from $(\alpha, xn\gamma)$†

D. G. McCauley* and J. E. Draper
Crocker Nuclear Laboratory,‡ University of California, Davis, California 95616
(Received 1 March 1971)

Ground-state band levels to 6^+ in ^{84}Kr, 6^+ in ^{82}Kr, 8^+ in ^{80}Kr, and 10^+ in ^{78}Kr have been identified with 20–65-MeV $(\alpha, xn\gamma)$ reactions on enriched Se targets with $x = 2$, 3, and 4. The data are in-beam and radioactive γ spectra, angular distributions, relative and absolute excitation functions and ~3-nsec time distributions. All transitions in the ground-state bands are ≳95% prompt (≲3 nsec) except for ^{84}Kr, in which the $6 \rightarrow 4$, $4 \rightarrow 2$, and $2 \rightarrow 0$ transitions have the same intensities of long-lived (≈200-nsec) component in addition to the prompt component. Multipole mixing ratios of three other transitions in ^{82}Kr are obtained from the angular distributions. The systematics of level energies in the ground-state bands of various Se, Kr, Mo, and Ru isotopes are analyzed with a phenomenological equation. This reveals three limiting types of nuclei.

I. INTRODUCTION

Prior to our earlier report,[1] very little was known about the ground-state quasirotational bands in even $_{36}$Kr nuclei. In ^{84}Kr the first 2^+ state was identified by radioactive decay[2] and by Coulomb excitation.[3,4] In ^{82}Kr 2^+ and 4^+ states were found.[2-9] In ^{80}Kr only the 2^+ state has been reported.[3,4,9] Very recently, levels to 6^+ were identified for ^{78,76}Kr, and to 4^+ for ^{74}Kr, from a (HI, $xn\gamma$) experiment.[10]

The systematic lowering of these first 2^+ states and enhancement of their $B(E2)$ values[4] with decreasing neutron number in even $_{36}$Kr isotopes is similar to the behavior of Te, Xe, Ba, and Ce nuclei occupying the nearby region $50 < Z < 82$ and $50 < N < 82$ of the nuclear chart.[9,11-14] The calculations of Marshalek, Person, and Sheline[15] suggested deformed regions, one near $_{52}$Te, $_{54}$Xe, $_{56}$Ba, and $_{58}$Ce and another near $_{34}$Se. They also noted that the weak shell closure at 40 neutrons or protons might provide enough rigidity to prevent deformation in that vicinity.

Experiments in this laboratory[13,14,16] and elsewhere[9-12,16,17] have shown quasirotational bands in $_{34}$Se, $_{42}$Mo, and $_{44}$Ru as well as $_{52}$Te, $_{54}$Xe, $_{56}$Ba, and $_{58}$Ce. It is then of interest to investigate experimentally the question whether these bands exist in $_{36}$Kr, and, if so, to investigate their relation to the bands of Se, Mo, and Ru.

II. EXPERIMENTAL METHOD

Most features of the experimental method have been described in previous reports,[13,14,16] and will not be repeated here. Briefly, the method is to measure the energy spectrum, angular distribution, and nanosecond timing distribution of the reaction γ rays produced by 25- to 65-MeV α particles in $(\alpha, xn\gamma)$ reactions. The α particles were produced by the Davis cyclotron in bunches with widths ≤2 sec when the cyclotron was properly adjusted. α particles of 20 MeV were obtained by degrading a 25-MeV beam with polyethylene placed just before the target. The γ detector was planar with active dimensions $0.75 \times 1.9 \times 1.9$ cm^3 and with resolution of 3.0 keV at 1332 keV.

All targets were selenium metal powder, supported by a 4-mm wide 0.88-mg/cm^2 strip of Mylar ($C_5H_4O_2$) and held in place on the Mylar by ~2 mg/cm^2 of Krylon plastic spray. The radiation from these supporting materials was small. The target impurities are listed in Table I, since they are needed to assess the spectra shown later. Excitation cross sections (absolute) were measured by using a target of natural selenium, whose area was much larger than the beam area. The 4-mm wide targets were so narrow that the beam could drift off them without proportionately affecting the current in the Faraday cup.

Most of the electronics used in this experiment has been described elsewhere.[13,14] "Walk" was reduced to ≤1.5 nsec over the interval 150 keV $< E^{\gamma} < 3000$ keV, by use of ORTEC units 453 and 454. Full widths at half maximum for the time-to-amplitude converter (TAC) spectra were typically 5 nsec at 150 keV and 1.5 nsec above 800 keV. The time-zero signal for the TAC was derived from the cyclotron dee voltage.

The γ yield was measured as a function of α energy for each isotope. These results were used for isotopic identification of each transition, for guidance in making level assignments, and for optimizing the ratio of the area of the γ-ray peak to the background for measurements of angular

TABLE I. Relative abundance of target impurities.

Nominal target	Isotope 76	77	78	80	82
^{76}Se	100	2.4	5.3	7.2	2.0
^{77}Se	2.1	100	4.8	6.7	1.4
^{78}Se	<1	<1	100	5.2	<1
^{80}Se	<1	<1	1.2	100	<1
^{82}Se	1.4	1.7	2.4	6.2	100

distributions and half-lives. The optimum beam energy for Se($\alpha, xn\gamma$)Kr to produce transitions between levels of high spin in the ground-state band is

$$E_\alpha^{\rm opt} = -Q + 9x \text{ MeV}, \qquad (1)$$

where Q is the threshold energy. The yields of $2 \to 0$ maximize about $1.5x$ MeV lower.

A problem with targets as light as selenium is that emission of charged particles can occur before γ emission. In particular, ($\alpha, np\gamma$) could compete with ($\alpha, 2n\gamma$), both producing prompt γ rays. This confuses the isotopic assignment of γ rays. As an *a priori* criterion for the probability of this contamination, the sum of the threshold energy for ($\alpha, np\gamma$) plus 18 MeV plus the Coulomb barrier for the outgoing proton was compared to Eq. (1) applied to ($\alpha, 2n\gamma$). This former sum was larger than the result of Eq. (1) by 10, 10, 12, and 13 MeV for targets of $^{76, 78, 80, 82}$Se, respectively; so the contamination by ($\alpha, np\gamma$) was expected to be negligible. This was confirmed by measurements of beam-induced radioactivity as discussed below.

Angular distributions were measured at 90, 110, 130, and 148°. As noted below, timing information for these angular distributions was only recorded in the 4096-channel analyzer when it was necessary in order to separate multiplet peaks with different half-lives.

III. EXPERIMENTAL RESULTS

Figure 1 summarizes the γ-ray spectra from $(\alpha, 2n\gamma)^{84, 82, 80, 78}$Kr and $(\alpha, 4n\gamma)^{76}$Kr. In order to focus the following discussions, Fig. 2 shows the level schemes for the ground-state bands, as deduced from the information about to be presented.

Figure 3 shows the ($\alpha, 2n\gamma$) relative excitation functions of the prompt component ($\lesssim$3 nsec) alone for transitions assigned to the ground-state bands. Normalization is to the respective $2 \to 0$ intensity. Figure 4 is the absolute excitation function of each of the $2 \to 0$ transitions for ($\alpha, 2n\gamma$) energies.

Figure 5 summarizes the angular distributions for transitions assigned to the ground-state bands. The curves for ^{76}Kr and for the "total" intensities of ^{84}Kr are least-squares fits to the data. All other curves of Fig. 5 result from the side-feeding method of analysis by Draper and Lieder.[18] The parity assignments in Fig. 2 are based on the assumption that all quadrupole transitions are electric.

A recurring problem was the presence of the 1013-keV γ ray from target-scattered α particles striking the aluminum beam pipe approximately

TABLE II. γ rays recorded from 25-MeV α particles on enriched ^{82}Se.

γ-ray energy (keV) [a]	Assignment	γ-ray cross section (mb) [b]	A_2, A_4 [c]	$T_{1/2}$ [d] (nsec)
424		194	−0.17(0.03), 0.09(0.04)	P
881	^{84}Kr $2 \to 0$	868	0.30(0.02), −0.01(0.03)	P
881	^{84}Kr $2 \to 0$	243	Assumed isotropic	LL
1012	^{84}Kr $2' \to 0$	20 [e]		P
1078	^{84}Kr $6 \to 4$	99	0.29(0.15), 0.01(0.22)	P
1078	^{84}Kr $6 \to 4$	204	Assumed isotropic	LL
1145		78 [f]	Too weak at 25 MeV	P
1122	^{83}Kr	112	−0.23(0.15), 0.38(0.21)	P
1214	^{84}Kr $4 \to 2$	284	0.28(0.07), 0.07(0.10)	P
1214	^{84}Kr $4 \to 2$	215	Assumed isotropic	LL
1464		260	0.25(0.07), −0.02(0.10)	P
1893	^{84}Kr $2' \to 0$	32	No data	P
1965		70	No data	48^{+206}_{-30}

[a] Uncertainties are 1.5 keV, unless otherwise stated.
[b] γ-ray cross sections in mb (uncorrected for angular distributions; uncertainties are $\lesssim$10%.
[c] Statistical uncertainties in the angular distribution coefficients A_2 and A_4 are in parentheses.
[d] A P denotes prompt ($\lesssim$3 nsec), while LL denotes long-lived ($\gtrsim$300 nsec).
[e] Deduced from ^{84}Kr 1893-keV $2^{+\prime} \to 0^+$ photopeak intensity and the branching ratio with the $2^{+\prime} \to 2^+$ from radioactivity.
[f] From a 30-MeV α-particle reaction on enriched ^{82}Se.

16 nsec beyond the target.[19] The proximity of the energy of this line to that of prompt transitions in the ^{78}Kr and ^{80}Kr spectra necessitated recording two-dimensional angular distributions (i.e., including timing) for these transitions. Because of the larger dead time of the analyzer in this mode and the extra complexity of analysis to compensate for drifts of the cyclotron beam bunching, these angular distributions are less precise. They are shown as hollow circles in Fig. 5 for 1015 keV in ^{78}Kr and for 1017 keV in ^{80}Kr.

The $6 \rightarrow 4$ 1099-keV transition in ^{82}Kr is in a multiplet with a weaker line at approximately 1097 keV, with a γ-ray intensity ratio of 4.5 for 25-MeV α particles; the precision of that angular distribution shown in Fig. 5 was reduced accordingly.

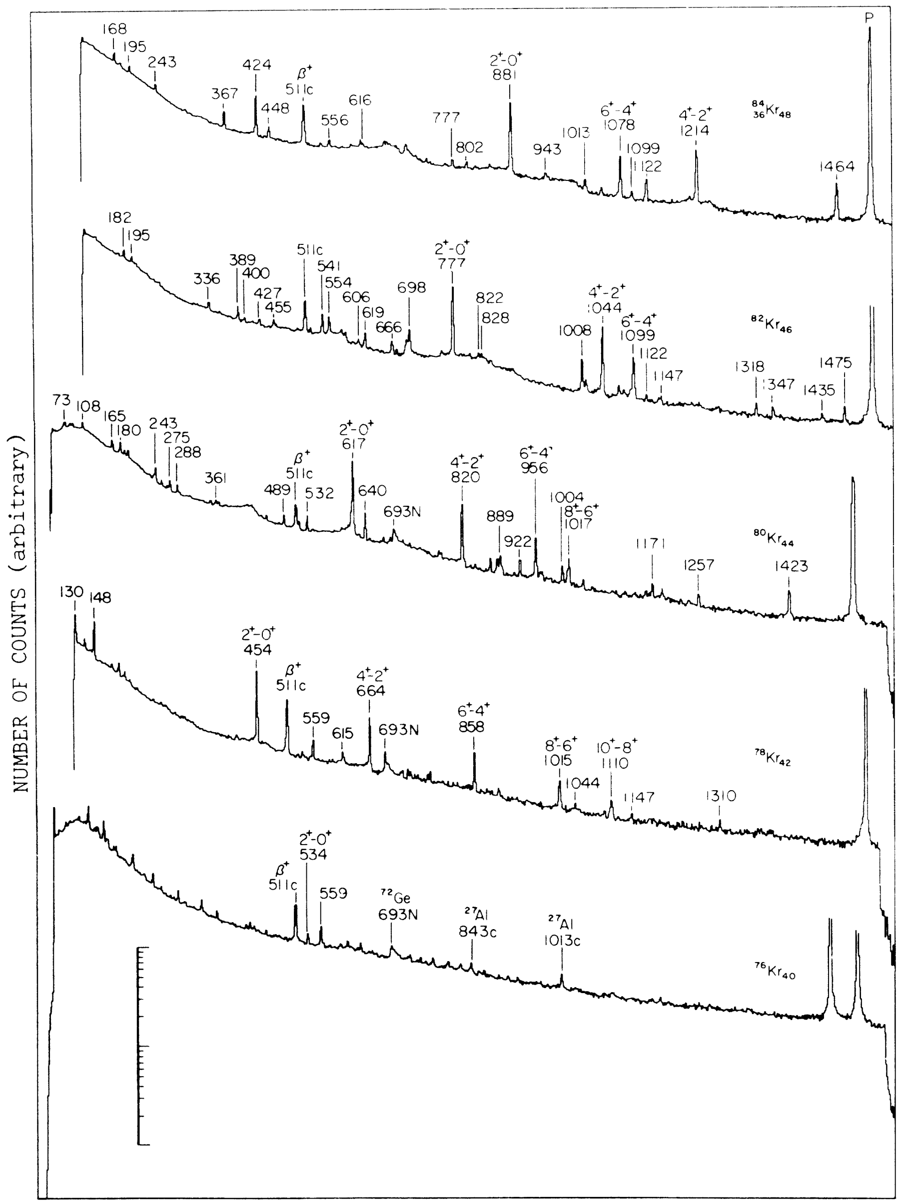

CHANNEL

FIG. 1. γ-ray spectra. From the top they are 25-MeV $(\alpha, 2n\gamma)^{84}$Kr, 25-MeV $(\alpha, 2n\gamma)^{82}$Kr, 25-MeV $(\alpha, 2n\gamma)^{80}$Kr, 30-MeV $(\alpha, 2n\gamma)^{78}$Kr, and 65-MeV $(\alpha, 4n\gamma)^{76}$Kr. The transitions assigned to the lowest $K=0$ bands are labeled by spin and parity. A two-decade log scale is inserted. Those peaks labeled c are common to several spectra; those peaks labeled N are from $(n, n')^{72}$Ge* and are also common to several spectra. The tall peaks at the right are pulser peaks, and they are truncated to avoid overlapping.

A. ^{84}Kr

Transitions from excited levels in ^{84}Kr have been studied previously by other workers using the radioactive decay of the 32-min ground state of $^{84}_{35}$Br and the 33-day ground state of $^{84}_{37}$Rb. Huddleston and Mitchell[2] placed the first excited state in ^{84}Kr at 0.890 MeV and assigned to it a spin and parity of 2^+. This assignment was supported by Temmer and Heydenburg[3] and by Heydenburg, Pieper, and Anderson[4] using Coulomb excitation. A second excited state at 1.91 ± 0.05 MeV with a $(1^+, 2^+)$ assignment was reported by Welker and Perlman[20] from the decay of ^{84}Rb. The most complete experiment to date on ^{84}Kr is that of Johnson and O'Kelley[21] from the decay of ^{84}Br. Bartholomew *et al.*,[22] in their compendium of the thermal-neutron-capture γ rays for $Z \lesssim 46$, report a transition of 1.23 ± 0.02 MeV from a level at 2.11 MeV to the 0.880-MeV 2^+ level. No spin or parity assignment was given to this 2.11-MeV level. The levels in ^{84}Kr published prior to the present work are summarized in the *Nuclear Data Sheets*[23] and by Lederer, Hollander, and Perlman,[9] hereafter called LHP.

The most intense γ rays recorded in beam and from beam-induced radioactivity are listed in Tables II and III. In Table II and similar ones, only the γ rays with relative intensities $\gtrsim 8\%$ of the $2 \to 0$ are included, unless they have been assigned. Of particular interest in this work are the transitions in the $K = 0$ ground-state band and those from the second excited 2^+ level in ^{84}Kr.

Figure 6 shows a two-parameter γ-ray spectrum of $(\alpha, 2n\gamma)^{84}$Kr at 25 MeV. Since ^{84}Se is not stable the $(\alpha, 4n\gamma)^{84}$Kr reaction could not be used for cross identification. The long-lived components of the $2 \to 0$, $4 \to 2$, and $6 \to 4$ transitions in ^{84}Kr were found to have the same intensity within 10% at 25 MeV. This equality was also found at 20, 30, and 35 MeV.

The 881-keV transition is the most intense in Table II and is taken as the $2^+ - 0^+$, in agreement with LHP. The absolute excitation function shown in Fig. 4 supports this agreement, as does the angular distribution in Fig. 5.

Assuming that the 881-keV transition in the radioactivity listed in Table III is from $(\alpha, pn)^{84}$Br β^- decay to ^{84}Kr, including the 32-min ^{84}Br of LPH

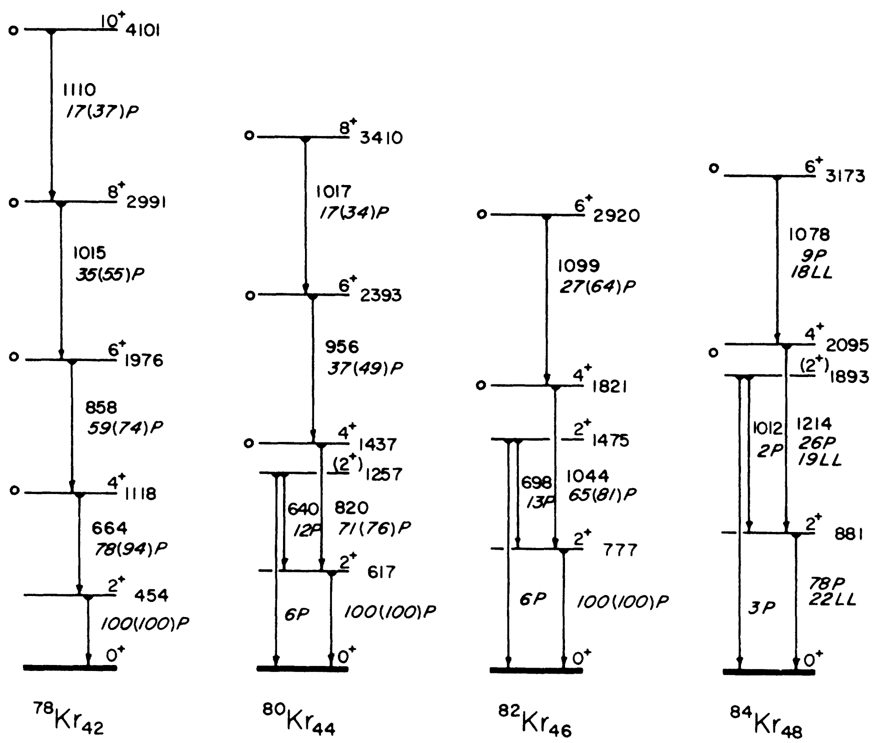

FIG. 2. Level scheme for the lowest $K = 0$ bands and second excited 2^+ states for the ^{78,80,82,84}Kr isotopes. Each transition shown is labeled with its energy in keV. The relative intensity for a $2n$ reaction is without parentheses, while that for a $4n$ reaction is within parentheses. A P denotes a prompt component relative intensity, while LL denotes long lived ($\gtrsim$300 nsec). Intensities for ^{78}Kr are from 30- and 65-MeV beams, those for ^{80,82}Kr are from 25- and 60-MeV beams and those for ^{84}Kr are from a 25-MeV beam. The small circle placed to the left of levels in the ground-state bands marks the level energy as calculated with the mathematical model discussed in Sec. IV.

and the 6-min ^{84}Br of Sattizahn *et al.*,[23,24] the data show that the cross section for $(\alpha, pn)^{84}$Br is only 0.0036 times that for $(\alpha, 2n\gamma)^{84}$Kr $(2 \rightarrow 0)$ at 25 MeV. Thus $(\alpha, pn\gamma)$ can be neglected as a source of γ rays in the prompt spectra, as expected from the discussion following Eq. (1).

The $4 \rightarrow 2$ and $6 \rightarrow 4$ transitions are assigned on the basis of the evidence in Tables II and III, and Figs. 3, 5–7. An important signature is that the $2 \rightarrow 0$, $4 \rightarrow 2$, and $6 \rightarrow 4$ all have the same intensity of delayed component within 10%, so they are in cascade. The other criteria have been discussed in our previous work.[13,14,16]

The equality of intensities of the long-lived components of $2 \rightarrow 0$, $4 \rightarrow 2$, and $6 \rightarrow 4$ and the lack of any other γ ray with a correspondingly large long-lived component means that the isomeric transition feeding the state of spin 6 must be very strongly internally converted and/or of energy below the approximately 80-keV threshold of the electronics in a run similar to that in Fig. 5. This will be considered below.

Transitions were sought from the second 2^+ level, shown in LHP at 1.90 MeV. A prompt transition near 1012 keV, a candidate for the $2' \rightarrow 2$, was most intense in the prompt band at 35 MeV, less intense at 30 MeV, and vanished in the statistics at 25 and 20 MeV. However, Fig. 4 shows that the $2 \rightarrow 0$ yield peaks at 25 MeV, so our 1012-keV transition has a maximum intensity at an α energy at least 10 MeV above the optimum for the $2 \rightarrow 0$. Data analysis for this transition is complicated by the 1013-keV line from ^{27}Al, whose yield peaks 16 nsecs downstream from the target.

Additional information about this $2^{+\prime}$ state stems from the radioactivity γ-ray spectrum in Fig. 7, recorded over a 22.4-min real time interval beginning 16 min after turning of the cyclotron beam; it shows the 1012- and 1893-keV γ rays. Table III shows that these transitions have the same branching ratio as the 1.01- and 1.90-MeV γ rays in LHP. Furthermore, the difference in energy of our 1893- and 1012-keV γ rays equals the energy of our 2^+ state, so we assign 1893 keV as $2^{+\prime} \rightarrow 0^+$ and 1012 keV as $2^{+\prime} \rightarrow 2^+$. In Fig. 12 there is only slight evidence of them in the prompt band.

There are many other transitions from ^{82}Se targets, some of whose properties are summarized in Table II. They will not be discussed further here, since they cannot yet be fitted into a level scheme. However, their properties (and those of unassigned transitions from other targets in tables to follow) are listed for diagnostic use and for possible use by other investigators.

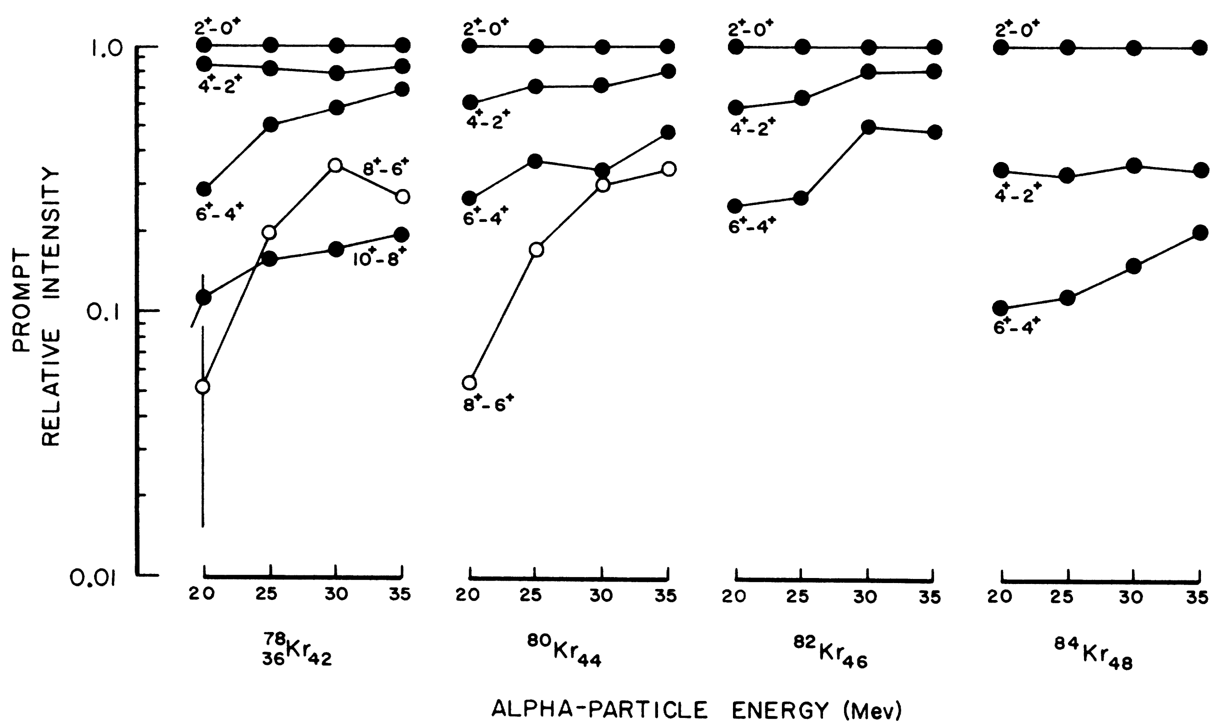

FIG. 3. Relative excitation functions of the prompt component for ^{78,80,82,84}Kr. Normalization is to the respective $2^+ \rightarrow 0^+$ transition. The hollow dots for the ^{78,80}Kr $8^+ \rightarrow 6^+$ transition intensities are reminders that these data were stripped from the 1013-keV ^{27}Al impurity lines, using two-parameter timing spectra.

B. ^{82}Kr

Transitions from excited levels in ^{82}Kr have been studied previously with the radioactive decay[5-7] of the 35-h 5^- ground state and 6.1-min 2^- isomeric state in $^{82}_{35}$Br, the 1.3-min 1^+ ground state and 6.4-h 5^- isomeric state[2,8] in $^{82}_{37}$Rb, Coulomb excitation experiments[3,4] and the ^{79}Br(α, p)-^{82}Kr reaction.[25,26] The positions of the 2^+, 4^+, and $2^{+\prime}$ levels are already established.

The γ rays recorded in beam from 25-MeV reactions on the enriched ^{80}Se target are shown in Fig. 8 and Table IV. Table IV also shows the characteristics of the ground-state band transitions for ($\alpha, 4n\gamma$) as well as ($\alpha, 2n\gamma$) reactions producing ^{82}Kr. As usual the ($\alpha, 4n\gamma$) has a larger relative production of higher-spin states than does ($\alpha, 2n\gamma$), but the ($\alpha, 4n\gamma$) spectra are not as clean in terms of ratios of peak height to background. The $2 \rightarrow 0$, $4 \rightarrow 2$, and $6 \rightarrow 4$ transitions as well as the $2' \rightarrow 2$ and $2' \rightarrow 0$ transitions are seen in Fig. 8 to be only prompt. That is, the counting rate for each of the $2 \rightarrow 0$, $4 \rightarrow 2$, and $6 \rightarrow 4$ transitions in the time band 10.1 to 21.1 nsec in Fig. 8 is smaller than that in the -3.1 to 3.5-nsec band by a factor $\lesssim 3 \times 10^{-3}$.

The spectrum of γ rays from beam-induced radioactivity is shown in Fig. 9, recorded over a 10.0-min real-time interval beginning 15 min after turning off the cyclotron. Analysis of these data show that if the only β^- decays of ^{82}Br originate from the 35-h and the 6.1-min levels[9] of ^{82}Br, then the ratio of 25-MeV in-beam counting rates of the ^{82}Kr $2 \rightarrow 0$ from ($\alpha, 2n\gamma$) compared with the ^{82}Kr $2 \rightarrow 0$ from (α, pn) β^- decay is 1600:1. Thus ($\alpha, pn\gamma$) can be ignored here for in-beam data.

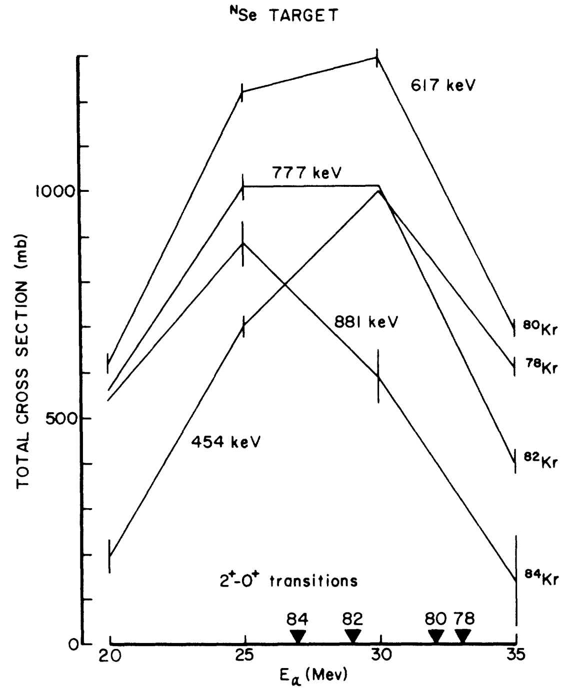

FIG. 4. Absolute excitation functions for the $2^+ \rightarrow 0^+$ measured with a natural Se target. Solid triangles on the energy axis mark the optimum beam energy for the ($\alpha, 2n\gamma$) reaction, as in Eq. (1). The curve for ^{84}Kr is for the prompt only component of $2 \rightarrow 0$. For ^{78}Kr the 35-MeV ($\alpha, 3n\gamma$)^{78}Kr reaction on the ^{77}Se impurity has been subtracted.

Whenever there is a pair of transitions from the same level, their angular distribution coefficients A_2, A_4 may yield the mixing ratio of one or both of them. If the magnetic substate population is exactly a Gaussian about $m = 0$ with a width σ, then

TABLE III. Radioactivity (if relative intensity >5%). The uncertainty in $E_\gamma = \pm 1.5$ keV; the uncertainty in $I_\gamma = \pm 10\%$ unless noted.

25 MeV ^{82}Se target		25 MeV ^{80}Se target		35 MeV ^{78}Se target		35 MeV ^{76}Se target	
E_γ	I_γ (%)	E_γ	I_γ (%)	E_γ	I_γ (%)	E_γ	I_γ (%)
306 [a]	19	511 [b]	107	208	8	134	17
424 [b]	26	529	18 ± 4	217	23	139	12
511 [b]	40	554 [b]	90	261	100	148 [b]	13
802 [b]	11	619 [b]	49	299	13	208	6
881 [b]	100	698 [b]	36	307	22	217	20
1012 [b]	12	777 [b]	100	389	12	261	100
1214 [b]	6 ± 2	828 [b]	47	397	73	299	14
1464 [b]	39	1044 [b]	37 ± 7	511 [b]	484	307	20
1893 [b]	19	1292	11 ± 4	547	11	389	12
2020	12	1318 [b]	32	606	63	397	62
2207	13 ± 3	1475 [b]	25 ± 4	617 [b]	115	511 [b]	483
2336	26 ± 4			666	21	606	36
				833	12 ± 3	615 [b]	25
						833	10

[a] Isomeric ^{85}Kr.

[b] Also appears in in-beam tables.

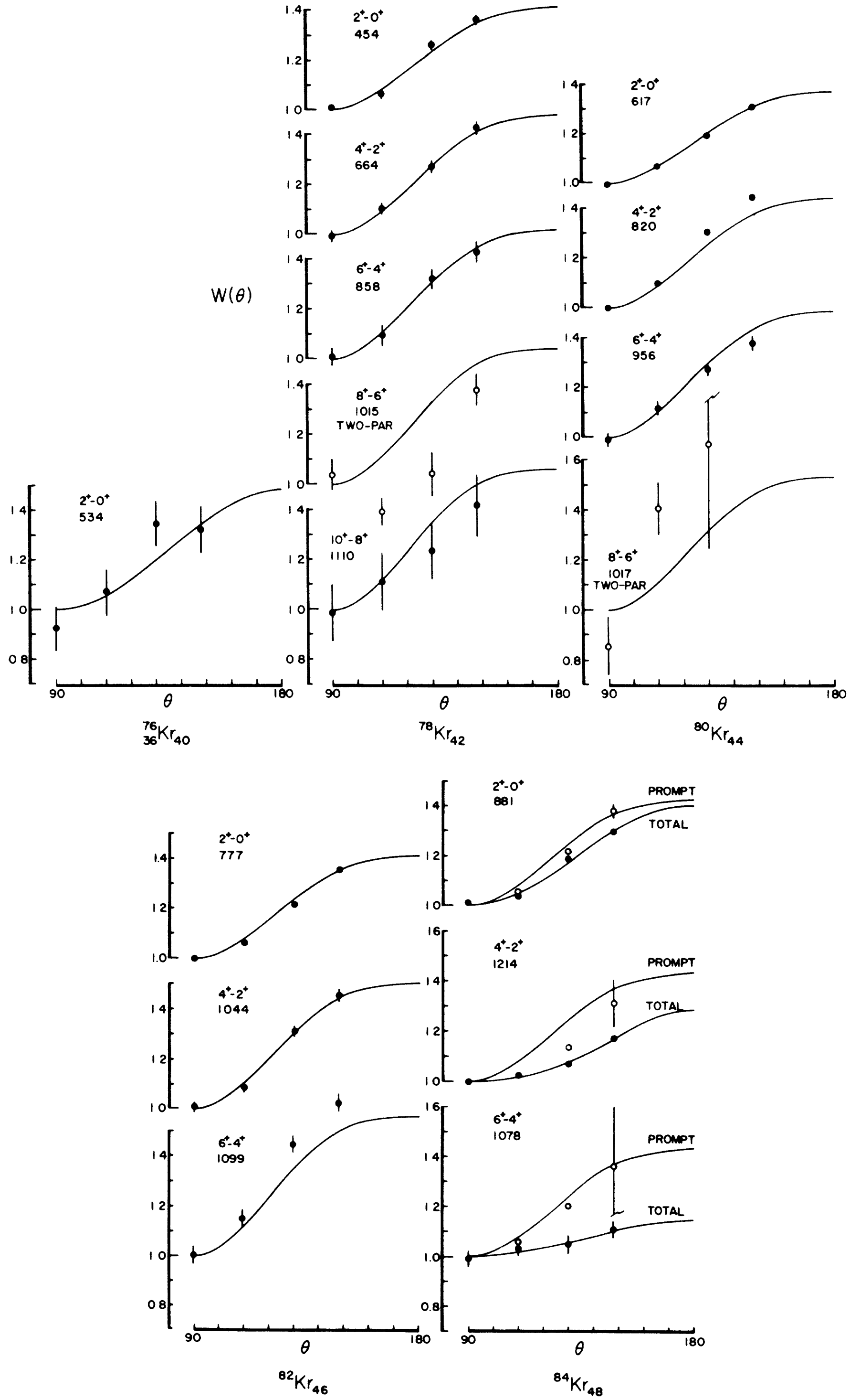

FIG. 5. Angular distributions for the lowest $K=0$ bands for the ^{76,78,80,82,84}Kr isotopes studied in this experiment. The data for the $8^+ \rightarrow 6^+$ transitions in ^{78,80}Kr are from two parameter angular distributions and are indicated by hollow dots. The curves for ^{76}Kr and those labeled TOTAL are least-squares fits to the data; all other curves are from the side-feeding intensity theory of Draper and Lieder (see Ref. 18). The Gaussian m-state populations as a function of spin are $\sigma = 0.7 + 0.3I$ for ^{84}Kr, $\sigma = 1.55 + 0.06I$ for ^{82}Kr, $\sigma = 1.7 + 0.1I$ for ^{80}Kr, and $\sigma = 1.84 + 0.1I$ for ^{78}Kr. The $6^+ \rightarrow 4^+$ 1099-keV transition in ^{82}Kr is in a multiplet (see text), which reduces the precision of the angular distribution. The error bars are only statistical.

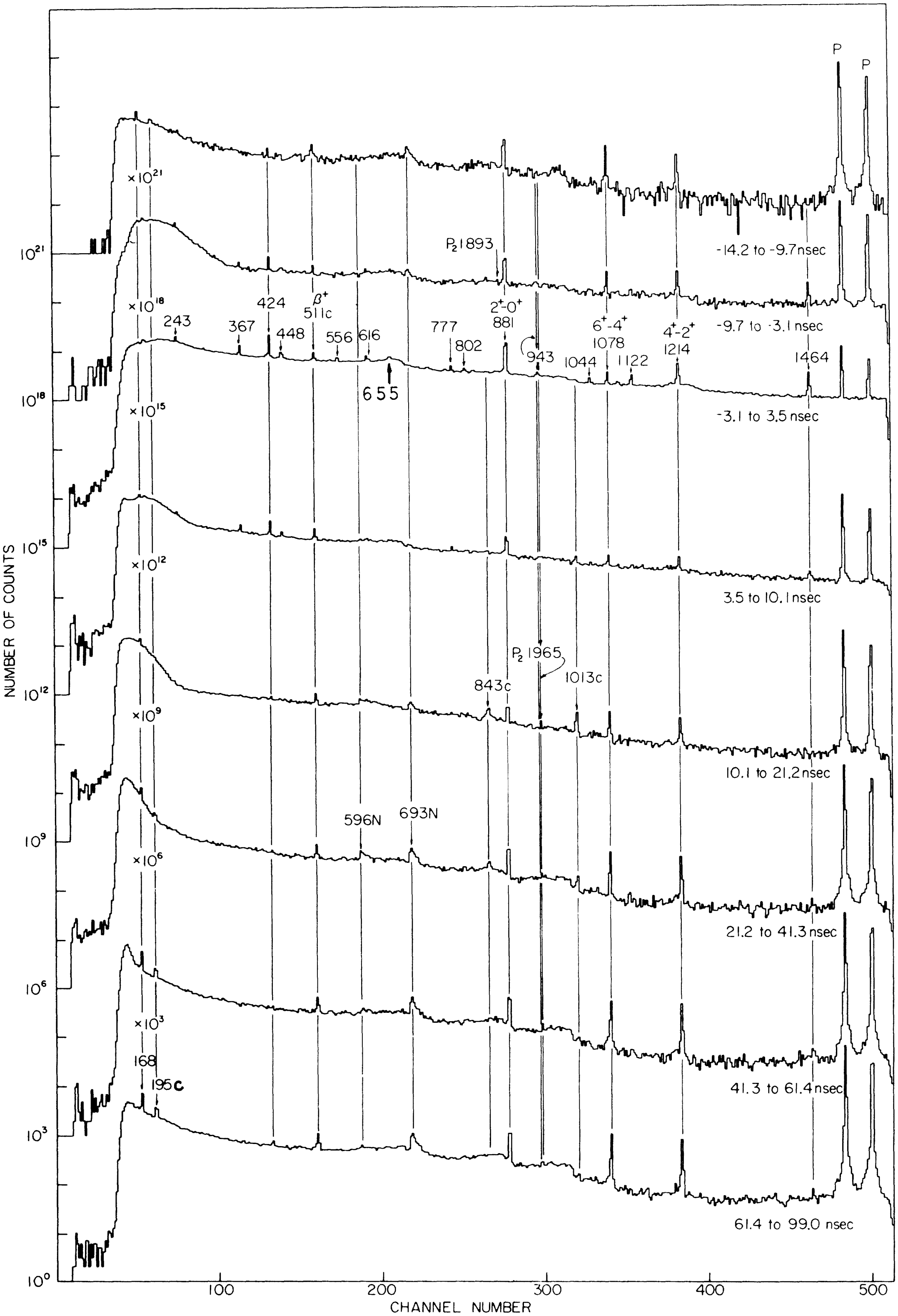

FIG. 6. γ spectra for a 25-MeV $(\alpha, 2n\gamma)^{84}$Kr reaction on enriched ^{82}Se. The eight time bands are shown separated by a factor of 10^3, and the time of each band with respect to the beam burst is given.

A_2, A_4 for a single transition can, in principle, provide σ and the mixing ratio δ. However, since the experimental A_4 has substantial experimental uncertainty, the angular distributions of each member of a pair of transitions from the same level can better be used to fix δ for one transition,[27] providing that δ for the other transition is already known. Such pairs of transitions in ^{82}Kr are $[2' \to 2$ (698 keV), $2' \to 0$ (1475)], $[3^+ \to 2'$ (619), $3^+ \to 2$ (1318)], and $[4^- \to 4^+$ (828), $4^- \to 3^+$ (554)], for in each case the mixing ratio of one member of the pair has been measured. Table V gives the mixing ratios obtained from the present angular distributions.

There has been considerable previous radioactivity work with ^{82}Kr. Figure 10 shows a summary of those levels obtained from 25-MeV in-beam γ rays investigated here. The excitation function for each of the two members of a pair of transitions from the same level is the same within uncertainties as required. Figure 8 shows that all of these transitions are prompt.

The fact that there are so few isomers in all of these Kr nuclei implies the smoothness of the curve of yrast levels.[28] That is, the energy of the lowest level of a given spin increases monotonically with spin so that there are no traps (or else they are not excited) to cause delayed γ rays.

The in-beam angular distributions of most of the transitions in Fig. 10 have been analyzed. There are no definitive conflicts with the assignments in Fig. 10; but additional work with, e.g., electron conversion coefficients and coincidences would help to complete the analysis.

C. ^{80}Kr

Previous information on ^{80}Kr levels is limited, since the only available radioactive decays were 1^+ ^{80}Br and 1^+ ^{80}Rb leading to states of low spin in ^{80}Kr. Only the 2^+ state at 618 keV was fairly certain.[3,4] There is a possible 0^+ state at 1320 keV.[23]

The in-beam γ spectrum with timing is not shown, since all but the 189-, 261-, and 275-keV γ rays are prompt. It also would show clearly a 1017-keV prompt γ ray that is distinct from the 1013-keV ^{27}Al γ ray appearing ~16 nsec down-

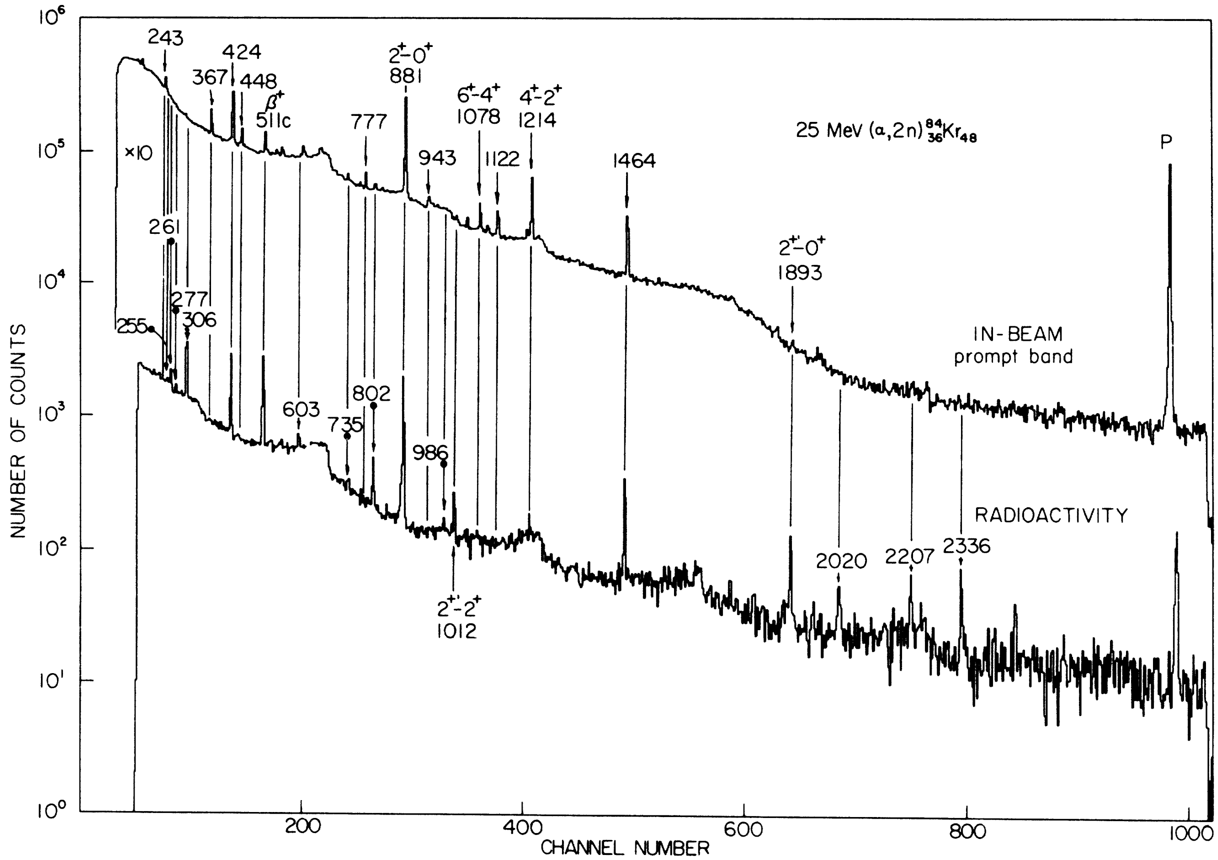

FIG. 7. The bottom spectrum is of beam-induced radioactivity following a 25-MeV $(\alpha, 2n\gamma)^{84}$Kr reaction on enriched ^{82}Se. It was recorded over a 22.4-min real-time interval (21.5-min live time), beginning 16 min after turning off the cyclotron beam. For comparison, the top spectrum shows the corresponding prompt band recorded in beam.

stream from the target. The characteristics of the γ rays are listed in Table VI.

The γ spectrum (not shown) from beam-induced radioactivity, taken over an interval of 20 min starting 15 min after turning off the cyclotron beam (35 MeV) shows that the ratio of $(\alpha, 2n\gamma)^{80}$Kr reactions to $(\alpha, pn\gamma)^{80}$Br reactions is 7.1, if there is no strong radioactive decay with half-life $\ll 15$ min. This ratio is estimated to be $\gtrsim 20$ at 25 MeV where the level assignments are made, since the $(\alpha, pn\gamma)$ cross section is expected to peak at ~42 MeV. Therefore $(\alpha, pn\gamma)$ prompt γ rays are negligible. The excitation functions of all γ rays assigned to ^{80}Kr are consistent with this isotopic assignment.

In addition to the ground-state band, there are assigned in Table VI the $2' \to 2$ (640 keV) and $2' \to 0$ (1257 keV). The branching ratio is 67% $(2' \to 2)$: 33% $(2' \to 0)$.

D. ^{78}Kr

Previous investigations of ^{78}Kr by Coulomb excitation[3,4] gave the first 2^+ state as 0.45 MeV. Very recently levels to 6^+ were reported[10] using (HI, $xn\gamma$).

Our in-beam timed spectra are not shown, since there are no delayed transitions except at 130, 148, and 206 keV. They also would show clearly a prompt 1015-keV γ ray in addition to the 1013-keV γ ray from ^{27}Al approximately 16 nsec downstream from the target. The characteristics of the γ rays are summarized in Table VII. In addition to ^{76}Se-$(\alpha, 2n\gamma)^{78}$Kr there were separately measured γ spectra from ^{77}Se$(\alpha, 3n\gamma)^{78}$Kr and ^{78}Se$(\alpha, 4n\gamma)^{78}$Kr and those results are also in Table VII. The similarity of results from $(\alpha, 2n\gamma)^{78}$Kr, $(\alpha, 3n\gamma)^{78}$Kr, and $(\alpha, 4n\gamma)^{78}$Kr makes certain the isotopic assignment of the intense lines at 454, 664, 858, 1015, and 1110 keV. The relative yield of higher-spin states is similar for $(\alpha, 2n\gamma)$ and $(\alpha, 3n\gamma)$ and larger for $(\alpha, 4n\gamma)$ in Table VII.

Concerning competing reactions, none of the lines in the spectrum of radioactivity is in the prompt band. Most of the radioactive γ rays can be assigned to β^+ decay of ^{79}Kr. This applies to both 25-MeV α particles on ^{76}Se and 35-MeV α particles on ^{77}Se, for which the spectra of radioactivity are almost the same. There is also a line in the radioactivity at 615 keV, and the only such γ ray expected (LHP) with significant intensity is from the decay of 6.5-min ^{78}Br produced by ^{76}Se(α, np). This target required the highest α energy to optimize $(\alpha, 2n)$, and has the lowest energy difference in the discussion following Eq. (1); so we expect the greatest competition from (α, np). Nevertheless, the transitions in Fig. 2 had the expected behavior of relative intensities for $(\alpha, 2n)$-^{78}Kr, $(\alpha, 3n)^{78}$Kr, and $(\alpha, 4n)^{78}$Kr, so they are believed to be correctly identified.

The properties of the $2^{+\prime}$ state in ^{78}Kr cannot be ascertained, since we cannot also use radioactive decay to ^{78}Kr.

The prompt transition at 559 keV is probably

TABLE IV. γ rays recorded from 25-MeV α particles on enriched ^{80}Se and 60-MeV α particles on ^{82}Se.

γ-ray energy (keV) [a]	Assignment	γ-ray cross section (mb) [b]	A_2, A_4 [c]	$T_{1/2}$ [d] (nsec)
		25-MeV α particles on ^{80}Se		
541		117	0.14(0.08), −0.09(0.12)	P
554	^{82}Kr $4^- \to 3^+$	84	−0.20(0.11), 0.00(0.16)	P
606	^{82}Kr $3^{()} \to 4^+$	38	0.50(0.25), 0.00(0.36)	P
619	^{82}Kr $3 \to 2$	88	0.30(0.11), 0.11(0.16)	P
698	^{82}Kr $2' \to 2$	128	0.20(0.08), 0.13(0.11)	P
777	^{82}Kr $2 \to 0$	1072	0.28(0.02), −0.02(0.02)	P
1008	^{82}Kr $(4, 5) \to 4$	162	−0.27(0.07), 0.03(0.11)	P
1044	^{82}Kr $4 \to 2$	689	0.32(0.02), −0.06(0.04)	P
1099	^{82}Kr $6 \to 4$	291	0.38(0.05), −0.13(0.07)	P
1318	^{82}Kr $3 \to 2$	50	0.48(0.22), 0.52(0.32)	P
1475	^{82}Kr $2' \to 0$	61	0.14(0.21), 0.06(0.30)	P
		60-MeV α particles on ^{82}Se		
777	^{82}Kr $2 \to 0$	100%	...	P
1044	^{82}Kr $4 \to 2$	81%	...	P
1099	^{82}Kr $6 \to 4$	64%	...	P

[a] Uncertainties are ±1.5 keV, unless otherwise stated.
[b] γ-ray cross sections in mb and not corrected for angular distributions; uncertainties are $\lesssim 10\%$.
[c] Statistical uncertainties in these angular distribution coefficients are in parentheses.
[d] A P denotes a prompt transition ($\lesssim 3$ nsec).

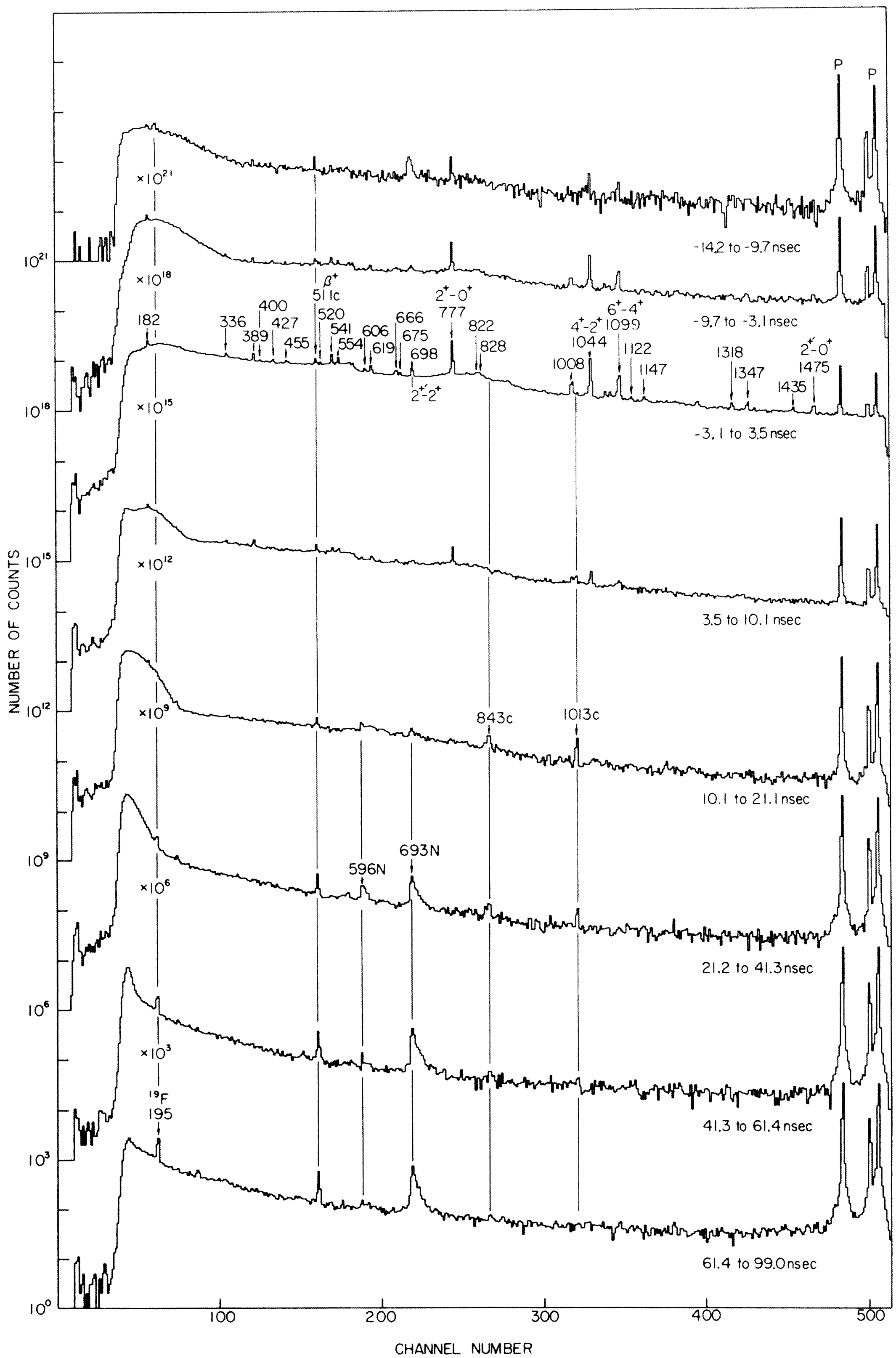

FIG. 8. γ spectra for a 25-MeV $(\alpha, 2n\gamma)^{82}$Kr reaction on enriched ^{80}Se.

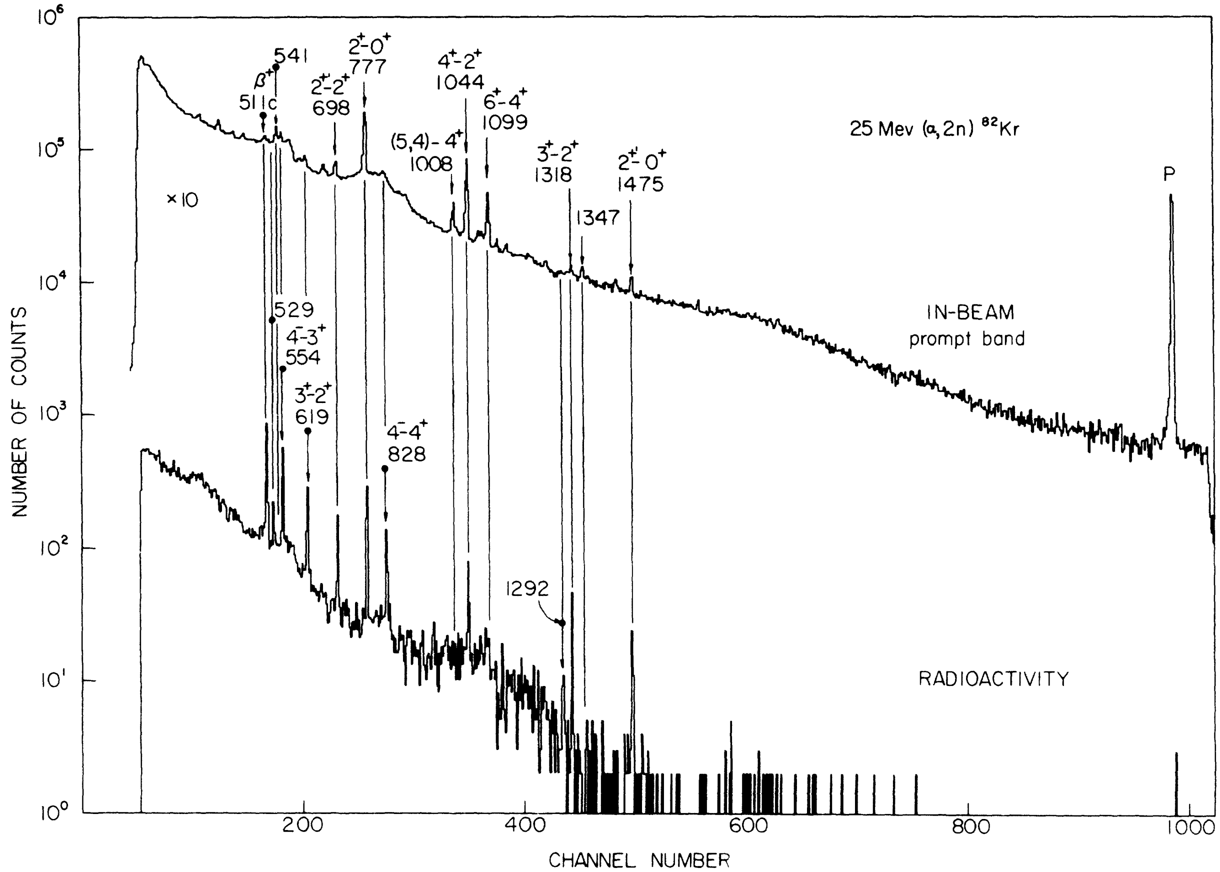

FIG. 9. The bottom spectrum is of beam-induced radioactivity following a 25-MeV $(\alpha, 2n\gamma)^{82}$Kr reaction on enriched ^{80}Se. It was recorded over a 10.0-min real-time interval (9.8-min live time), beginning 15 min after turning off the cyclotron beam. For comparison, the top spectrum shows the corresponding prompt band recorded in beam.

TABLE V. Mixing ratios for transitions in ^{82}Kr.

γ-ray energy (keV)	Assignment	This work[a] A_2	This work[a] σ	This work[a] δ	Other work: Gupta et al.[b] $\lvert\delta\rvert$	Other work: Meredith et al.[c] $\lvert\delta\rvert$	Other work: Etherton et al.[d] $\lvert\delta\rvert$
554	$4^- \rightarrow 3^+$	-0.20 ± 0.11	$1.2^{+1.5}_{-1.2}$	$0.06^{+0.05}_{-0.06}$	$0(E1)$	$0(M1)$	$0.0 \pm 0.1(E1)$
619	$3^+ \rightarrow 2^+$	0.30 ± 0.11	$1.02^{+0.68}_{-1.02}$	10^{+90}_{-8}	2.34 ± 0.05	$0(M1)$	2.0 ± 0.3
698	$2^{+\prime} \rightarrow 2^+$	0.20 ± 0.08	$1.7^{+\infty}_{-0.7}$	$1.0^{+3.0}_{-1.0}$	2.2 ± 0.9	$\infty(E2)$	3.0 ± 0.7

[a] $\delta = \langle \| L=2 \| \rangle / \langle \| L=1 \| \rangle$, where $\delta^2 = I_2^\gamma / I_1^\gamma$; σ is the Gaussian width of m states for the emitting level.

[b] See Ref. 5.

[c] Pure multipolarities were assumed (see Ref. 7).

[d] See Ref. 26.

Coulomb excitation of the 2^+ in the target ^{76}Se; this is also supported by the rather flat excitation function. More broadly, the data are consistent with 70–150 mb of Coulomb excitation of each of the even Se targets at approximately 25 MeV; for the ^{78}Se target the Coulomb excitation at 614 keV is masked by the 10 times stronger 617-keV $2\to 0$ in ^{80}Kr.

E. ^{76}Kr

Levels to 6^+ in ^{76}Kr have been reported quite recently from (HI, $xn\gamma$) reactions.[10] The less favorable $(\alpha, 4n\gamma)$ reaction was required to produce it in our work since a separated ^{74}Se target was too costly. The estimated optimum energy for $2\to 0$ is 66 MeV; 60- and 65-MeV α particles were used. At 60 MeV, the only significant peaks in the prompt band in the region above approximately 350 keV are the 511, 534, and 559 keV. The prompt component of the 559 keV is most probably Coulomb excitation of the target ^{76}Se, as observed also at low α energies. The radioactivity spectrum showed strong lines at 511, 559, 658, and 1216 keV, which correspond well with ^{76}Br-$(\beta^+)^{76}$Se from ^{76}Se$(\alpha, 3np)^{76}$Br. The latter three lines are $2\to 0$, $2'\to 0$, and $2'\to 0$ in ^{76}Se.[9] It would appear that the prompt 534 keV (no delayed component) might be the $2^+\to 0^+$ in ^{76}Kr. Its angular distribution in Fig. 5 is satisfactory for the $2\to 0$.

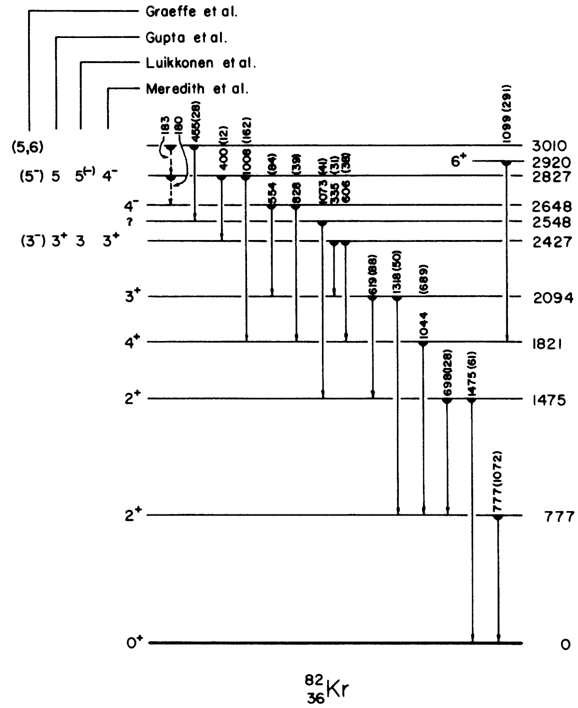

FIG. 10. Level scheme for ^{82}Kr. Numbers in parentheses are our cross sections in mb at 25 MeV.

TABLE VI. γ rays recorded from 25-MeV α particles on enriched ^{78}Se and 60-MeV α particles on ^{80}Se.

γ-ray energy (keV) [a]	Assignment	γ-ray cross section (mb) [b]	A_2, A_4 [c]	$T_{1/2}$ [d] (nsec)
		25-MeV α particles on ^{78}Se		
532		92	0.41(0.10), 0.16(0.14)	P
617	^{80}Kr $2\to 0$	1215	0.23(0.01), −0.03(0.02)	P
640	^{80}Kr $2'\to 2$	146	0.07(0.05), 0.08(0.07)	P
820	^{80}Kr $4\to 2$	862	0.31(0.02), −0.07(0.03)	P
889		136	0.38(0.07), 0.14(0.10)	P
922	^{81}Kr	85	0.34(0.13), 0.01(0.18)	P
956	^{80}Kr $6\to 4$	447	0.25(0.04), −0.11(0.05)	P
1004		94	−0.44(0.15), −0.19(0.21)	P
1017	^{80}Kr $8\to 6$	206	0.74(0.62), ⋯	(P) [e]
1257	^{80}Kr $2'\to 0$	72	0.07(0.19), −0.06(0.28)	P
1423		126	−0.28(0.16), 0.15(0.23)	P
		60-MeV α particles on ^{80}Se		
617	^{80}Kr $2\to 0$	100%	⋯	P
820	^{80}Kr $4\to 2$	76%	⋯	P
956	^{80}Kr $6\to 4$	49%	⋯	P
1017	^{80}Kr $8\to 6$	34%	⋯	(P) [e]

[a] Uncertainties are ±1.5 keV, unless otherwise stated.
[b] γ-ray cross sections are in mb and not corrected for angular distributions; uncertainties are $\lesssim$10%.
[c] Statistical uncertainties in the angular distribution coefficients A_2 and A_4 are in parentheses.
[d] A P denotes a prompt transition ($\lesssim$3 nsec).
[e] Although there is negligible LL component, any short delay would be masked by the 1013-keV line in ^{27}Al.

TABLE VII. γ rays recorded from 30-MeV α particles on enriched ^{76}Se, 35-MeV α particles on ^{77}Se, and 65-MeV α particles on ^{78}Se.

γ-ray energy (keV) [a]	Assignment	γ-ray cross section (mb) [b]	A_2, A_4 [c]	$T_{1/2}$ [d] (nsec)
		30-MeV α particles on ^{76}Se		
148 [e,f]		236	0.01(0.02), −0.07(0.02)	LL
454	^{78}Kr $2^+ \to 0^+$	990	0.26(0.02), −0.06(0.03)	P
559		127	0.00(0.10), 0.15(0.14)	P
664	^{78}Kr $4^+ \to 2^+$	775	0.31(0.03), −0.05(0.04)	P
777		99	0.25(0.16), −0.05(0.23)	P
858	^{78}Kr $6^+ \to 4^+$	558	0.29(0.05), −0.10(0.07)	P
1015	^{78}Kr $8^+ \to 6^+$	348	0.46(0.16), 0.34(0.24)	(P) [g]
1110	^{78}Kr $10^+ \to 8^+$	169	0.31(0.15), 0.02(0.21)	P
		35-MeV $^{77}Se(\alpha, 3n)^{78}Kr$		
454	$2 \to 0$	100%	...	P
664	$4 \to 2$	84%	...	P
858	$6 \to 4$	53%	...	P
1015	$8 \to 6$	28%	...	(P) [g]
1110	$10 \to 8$	15%	...	P
		65-MeV $^{78}Se(\alpha, 4n)^{78}Kr$		
454	$2 \to 0$	100%	...	P
664	$4 \to 2$	94%	...	P
858	$6 \to 4$	74%	...	P
1015	$8 \to 6$	55%	...	(P) [g]
1110	$10 \to 8$	37%	...	P

[a] Uncertainties are ±1.5 keV, unless otherwise stated.
[b] γ-ray cross sections are in mb and not corrected for angular distributions; uncertainties are $\lesssim$10%.
[c] Statistical uncertainties in the angular distribution coefficients A_2 and A_4 are in parentheses.
[d] A P denotes a prompt transition ($\lesssim$3 nsec), while a LL denotes long lived.
[e] A transition of this energy is also recorded at the 65-MeV $(\alpha, 4n)^{78}Kr$ reaction energy.
[f] From more than one reaction.
[g] Although there is negligible LL component, any short delay would be masked by the 1013-keV line in ^{27}Al.

However, we cannot check this with other reactions as was done for the other Kr isotopes.

The same results were obtained at 65 MeV, but the intensity of the 534-keV line was only 0.5 as large relative to the Coulomb excited 559 keV as at 60 MeV. It was not possible to measure the excitation function from the natural Se target bombardment. The assignment of a 424-keV γ ray as $2 \to 0$ in Ref. 10 should be more definitive for this particular case where we could only do an $(\alpha, 4n)$ reaction; but it is not clear why the 424-keV line did not appear in our $(\alpha, 4n)$ spectra, unless the $(\alpha, 3np)$ dominated the $(\alpha, 4n)$.

IV. PHENOMENOLOGICAL SYSTEMATICS OF GROUND-STATE BANDS

There are no detailed microscopic theories of these Kr nuclei that have given good numerical results. Kisslinger and Sorenson[29] have noted that for $28 \leq Z \leq 50$, $28 \leq N \leq 50$ there is a high probability of neutrons and protons occupying the same j shell and a consequent need for including the short-range neutron-proton interaction in calculations. Better treatments of proton and pairing vibrations are also needed for these nuclei.[30,31] Previous theoretical results yielded level schemes intermediate between stiff rotors, whose level energies are proportional to $I(I+1)$, and pure vibrators, whose level energies are equally spaced. In the Kr nuclei Fig. 2 shows patterns ranging from somewhat rotational in ^{78}Kr, with level spacings monotonically increasing, to the other extreme of ^{84}Kr where the $I = 0^+, 2^+, 4^+, 6^+$ level spacing increases and then decreases. We have also observed this in ^{120}Te compared[14] with ^{126}Te and in ^{74}Se compared[16] with ^{78}Se.

These smoothly varying patterns of levels can be described very nicely with a phenomenological equation. There have been several such equations, but one of us has recently outlined the basis for deriving them on quite general grounds without perturbative treatment and has interrelated them.[32] In that report it is shown that the same differen-

TABLE VIII. Nuclear-model numbers for even isotopes of Se, Kr, Mo, and Ru. All experimental E_γ are measured to approximately ±1.5 keV or better.

		$2^+\rightarrow 0^+$	$4^+\rightarrow 2^+$	$6^+\rightarrow 4^+$	$8^+\rightarrow 6^+$	$10^+\rightarrow 8^+$	$12^+\rightarrow 10^+$	$14^+\rightarrow 12^+$	N_b	H_b	$\mathscr{I}_0$ (keV^{-1})	$\mathscr{I}_{16}$ (keV^{-1})	$\langle(\Delta X_b)^2\rangle^{1/2}$ (%)
$^{72}_{34}$Se	E_{exp}[a]	862	775	830									
	E_{calc}	862	789	802	811	819	825	830	1.9	1.5(−3)	1.1(−4)	0.039	0.80%
	$\mathscr{I}_I/\mathscr{I}_0$	58.0	102.6	146.2	189.2	231.8	274.1	316.2					
^{74}Se	E_{exp}[a]	635	728	868	966								
	E_{calc}	635	753	849	922	980	1031	1074	1.2	4.8(−3)	5.7(−4)	0.029	1.4
	$\mathscr{I}_I/\mathscr{I}_0$	12.6	19.5	25.5	31.1	36.4	41.4	46.2					
^{76}Se	E_{exp}[a]	560	772	932	1008	1131							
	E_{calc}	560	774	918	1029	1121	1201	1271	1.0	7.9(−2)	2.9(−3)	0.024	0.53
	$\mathscr{I}_I/\mathscr{I}_0$	3.7	5.4	6.8	8.0	9.2	10.3	11.3					
^{78}Se	E_{exp}[a]	613	886	1040	1036								
	E_{calc}	613	889	1004	1071	1116	1149	1175	2.0	5.9(0)	3.3(−3)	0.027	1.1
	$\mathscr{I}_I/\mathscr{I}_0$	1.9	2.9	3.8	4.8	5.7	6.6	7.5					
$^{76}_{36}$Kr	E_{exp}[b]	424	610	824									
	E_{calc}	424	634	783	902	1004	1094	1175	0.8	6.8(−2)	3.0(−3)	0.026	2.5
	$\mathscr{I}_I/\mathscr{I}_0$	3.0	4.1	5.0	5.8	6.6	7.2	7.8					
^{78}Kr	E_{exp}[c]	454	664	858	1015	1110							
	E_{calc}	454	679	849	989	1111	1220	1319	0.7	7.4(−3)	1.9(−3)	0.023	0.94
	$\mathscr{I}_I/\mathscr{I}_0$	4.5	6.0	7.3	8.3	9.3	10.2	11.0					
^{80}Kr	E_{exp}[c]	617	820	956	1017								
	E_{calc}	617	823	942	1028	1096	1152	1201	1.3	3.5(−1)	2.1(−3)	0.026	0.42
	$\mathscr{I}_I/\mathscr{I}_0$	3.2	4.8	6.2	7.6	8.8	10.1	11.2					
^{82}Kr	E_{exp}[c]	777	1044	1099									
	E_{calc}	777	1041	1096	1106	1102	1091	1079	3.7	2.1(1)	2.5(−3)	0.031	0.13
	$\mathscr{I}_I/\mathscr{I}_0$	2.0	3.3	4.7	6.2	7.7	9.2	10.8					
^{84}Kr	E_{exp}[c]	881	1214	1078									
	E_{calc}	881	1168	1151	1086	1019	957	902	>30	>2.3(3)	2.4(−3)	0.040	2.2
	$\mathscr{I}_I/\mathscr{I}_0$	1.8	3.2	4.8	6.7	8.9	11.2	13.8					
$^{92}_{42}$Mo	E_{exp}[d]	1511	773	330	147								
	E_{calc}	1511	671	498	405	346	304	272	>30	5.5(0)	7.0(−5)	0.14	3.1
	$\mathscr{I}_I/\mathscr{I}_0$	87.7	229.3	420.2	656.0	933.6	1251.0	1606.5					
^{94}Mo	E_{exp}[e]	870	702	849									
	E_{calc}	870	753	737	726	717	709	703	2.4	2.3(−2)	2.4(−4)	0.048	3.0
	$\mathscr{I}_I/\mathscr{I}_0$	3.9	5.1	6.0	6.7	7.4	7.9	8.5					
^{96}Mo	E_{exp}[e]	778	850	813	929								
	E_{calc}	778	837	864	877	885	889	892	2.2	4.8(−1)	1.1(−3)	0.037	1.4
	$\mathscr{I}_I/\mathscr{I}_0$	2.2	2.8	3.2	3.6	4.0	4.3	4.6					
^{98}Mo	E_{exp}[e]	788	723	834									
	E_{calc}	788	751	775	791	804	815	823	1.8	2.9(−3)	1.8(−4)	0.040	1.8
	$\mathscr{I}_I/\mathscr{I}_0$	38.0	65.9	92.8	119.2	145.2	170.8	196.2					
^{104}Mo	E_{exp}[f]	192.3 ± 0.5	369	520									
	E_{calc}	192.3	369	519	656	783	903	1017	0.3	3.5(−2)	1.1(−2)	0.03	0.1
	$\mathscr{I}_I/\mathscr{I}_0$	1.6	1.8	2.0	2.1	2.2	2.4	2.4					
^{106}Mo	E_{exp}[f]	172	351	512									
	E_{calc}	172	351	511	661	803	940	1073	0.2	3.2(−2)	1.4(−2)	0.03	0.1
	$\mathscr{I}_I/\mathscr{I}_0$	1.3	1.5	1.6	1.6	1.7	1.8	1.8					
$^{94}_{44}$Ru	E_{exp}[d]	1428	755	311	143								
	E_{calc}	1428	652	486	397	339	298	268	>30	>6.9(0)	8.6(−5)	0.14	3.3
	$\mathscr{I}_I/\mathscr{I}_0$	73.3	190.4	347.9	542.0	770.5	1031.4	1323.4					

TABLE VIII *(Continued)*

		$2^+\to 0^+$	$4^+\to 2^+$	$6^+\to 4^+$	$8^+\to 6^+$	$10^+\to 8^+$	$12^+\to 10^+$	$14^+\to 12^+$	N_b	H_b	$\mathcal{J}_0$ (keV^{-1})	$\mathcal{J}_{16}$ (keV^{-1})	$\langle(\Delta X_b)^2\rangle^{1/2}$ (%)
^{96}Ru	E_{exp} [e]	832	686	632	801								
	E_{calc}	832	698	680	667	658	650	643	2.4	9.8(−3)	1.7(−4)	0.052	2.1
	$\mathcal{J}_I/\mathcal{J}_0$	41.7	77.9	114.9	152.7	191.1	230.0	269.4					
^{98}Ru	E_{exp} [e]	653	746	825	904								
	E_{calc}	653	751	827	882	925	961	992	1.4	2.9(−2)	8.3(−4)	0.032	0.4
	$\mathcal{J}_I/\mathcal{J}_0$	8.6	13.7	18.3	22.7	26.8	30.9	34.8					
^{100}Ru	E_{exp} [e]	540	688	850	985								
	E_{calc}	540	713	838	934	1015	1085	1147	1.0	1.6(−2)	1.3(−3)	0.027	1.6
	$\mathcal{J}_I/\mathcal{J}_0$	6.0	8.8	11.2	13.3	15.2	17.1	18.8					
^{102}Ru	E_{exp} [e]	476	632	768									
	E_{calc}	476	639	754	843	916	980	1037	1.0	3.4(−2)	1.8(−3)	0.030	0.7
	$\mathcal{J}_I/\mathcal{J}_0$	4.8	7.0	8.9	10.5	12.1	13.5	14.9					
^{110}Ru	E_{exp} [f]	241	423	576									
	E_{calc}	241	424	575	708	830	943	1050	0.4	3.9(−3)	5.6(−3)	0.03	0.1
	$\mathcal{J}_I/\mathcal{J}_0$	2.6	3.2	3.6	4.0	4.2	4.5	4.7					

[a] See Ref. 16.
[b] See Ref. 10.
[c] Data from this work.
[d] See Ref. 38.
[e] See Ref. 17.
[f] See Ref. 39.

tial equation which leads to the Harris formula[33] also leads to an equivalent expression of the form

$$E=\sum_{i,j=1}^{m} C_{ij}(x_i-x_{i0})(x_j-x_{j0})$$

$$+\sum_{i=1}^{m} D_i(x_i-x_{i0})+\frac{I(I+1)}{2\mathcal{J}(x_1,\ldots,x_n)} \tag{2}$$

subject to

$$\partial E/\partial x_i=0 \quad i=1,\ldots,m \tag{3}$$

interpreted as locating the *minimum* of E. In Ref. 32 the linear sum is omitted, but Eq. (2) is a useful generalization. The combination of Eqs. (2) and (3) gives the level energy E for spin I, given the functional form of the "moment of inertia" $\mathcal{J}(x_1,\ldots,x_m)$. The variables x_i are quadrupole deformation of the nucleus, neutron-proton pairing, neutron-neutron pairing, proton-proton pairing, a purely rotational parameter, and possibly others. Equations (2) and (3) may be reduced by algebraic substitution to a one-dimensional equation

$$E=\alpha_1(y-y_0)^2+\alpha_2+\frac{I(I+1)}{2\mathcal{J}(y)} \tag{4}$$

subject to

$$\frac{\partial E}{\partial y}=0\,. \tag{5}$$

Here α_1 depends on the C_i's but does not depend on the D_i's, while α_2 depends on both C_i and D_i and vanishes if each $D_i=0$.

A reasonable phenomenological choice of the functional form of the "moment of inertia" is

$$\mathcal{J}=\gamma y_I^N\,, \tag{6}$$

since Eq. (6) can approximate a variety of physically reasonable shapes. The case $N=1$ is the variable-moment-of-inertia (VMI) model.[34–36] A more detailed analysis of Eqs. (4)–(6) with arbitrary N has been made.[37]

We have found $N=1$ to be too restrictive for these Kr nuclei, so they have been analyzed with the N that provides the best fit to experiment. Only the ground-state band is available, so $\alpha_2=0$ in Eq. (4).

Equations (4) and (5) can be rewritten as

$$\epsilon_I=\{H(1-\zeta_I)^2+I(I+1)/\zeta_I^N\}_{\min}\,, \tag{7a}$$

where the definitions are

$$\epsilon_I=E_I\,2\gamma\,y_0{}^N=2E_I\mathcal{J}_0\,, \tag{7b}$$

$$H=2\gamma\alpha_1 y_0{}^{N+2}=\mathcal{J}_0 2\alpha_1 y_0{}^2\,, \tag{7c}$$

$$\zeta_I=y_I/y_0\,, \tag{7d}$$

and I is the angular momentum of the level in question. The subscript I denotes the equilibrium value for level I. The constants H and N are obtained from the best fits to experimental level energies. Thus for a given H and N there is a ζ_I which minimizes the bracketed quantity in Eq. (7a) for $I=2$. The E_2 experimental energy determines the corresponding $\mathcal{J}_0$ from Eq. (7b). These $\mathcal{J}_0$, H, and N are then used in Eq. (7a) successively with $I=4, 6, \ldots,$ to obtain the predicted E_4, E_6,

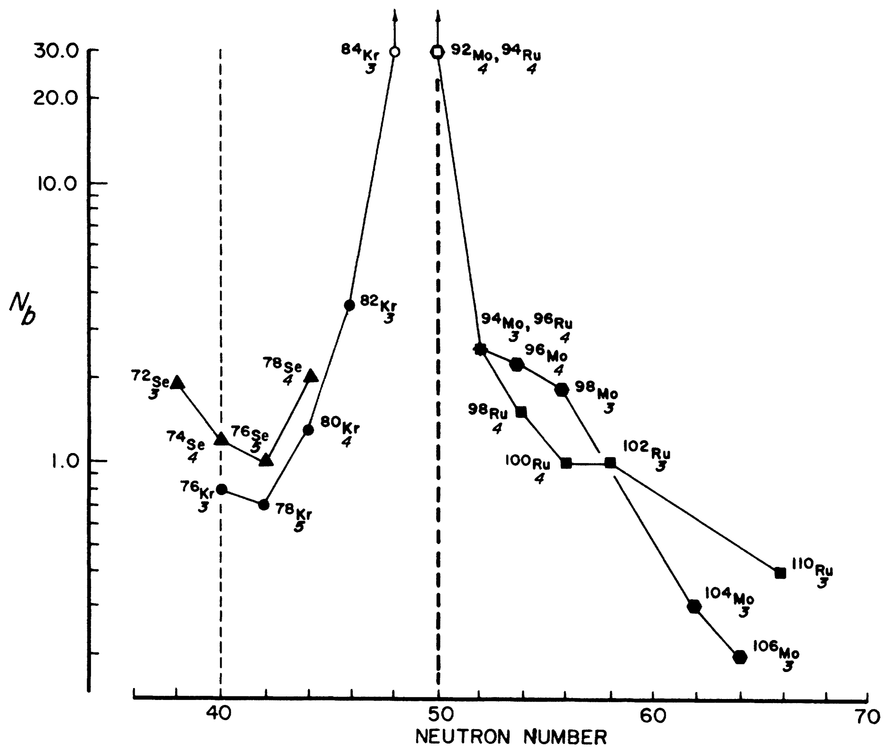

FIG. 11. Best parameter N_b for Se, Kr, Mo, and Ru. The hollow symbols at 48 and 50 neutrons indicate that $N > 30$ is preferred. The number listed at each point is the number of experimental transitions available for comparison with the model calculation. The lighter vertical dashed line at neutron number 40 marks the minor shell closure.

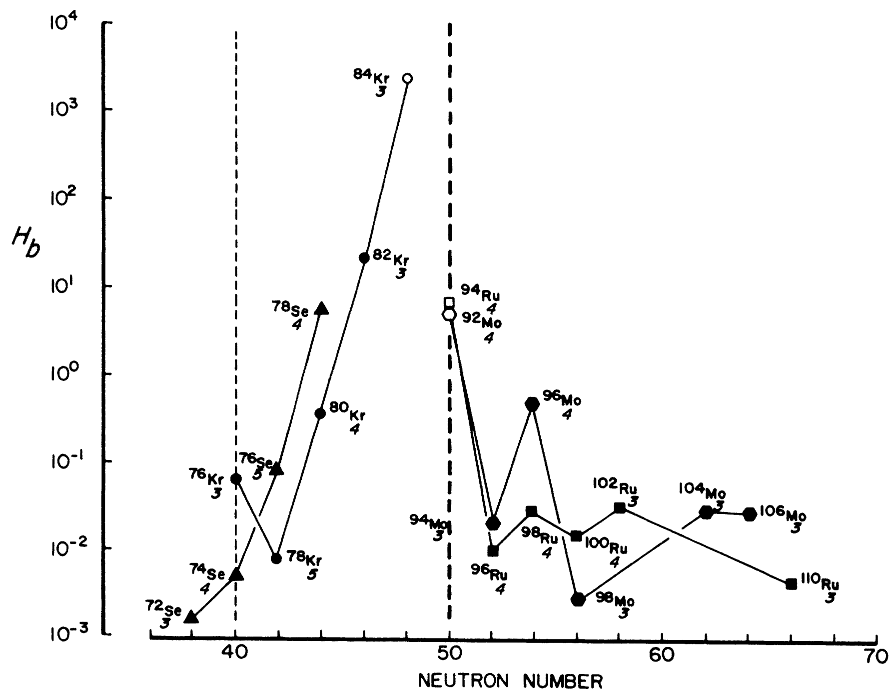

FIG. 12. Best parameters H_b corresponding to Fig. 11.

... for comparison with the experimental values. A systematic computer search was made through values of N and H to determine the best constants N_b and H_b for the nucleus in question. If one chooses always to fit the experimental E_2 energy exactly, then Eq. (7a) is a two-parameter equation for fitting E_4/E_2, E_6/E_2, ...

For the present data we chose to analyze γ-ray energies rather than level energies, since the uncertainties in the former are not cumulative over the levels beneath the one in question. The criterion for best values N_b and H_b was minimum, unweighted rms deviation from experiment of the normalized transition energy, defined as

$$X_I = \frac{(E_I - E_{I-2})/[I(I+1) - (I-2)(I-2+1)]}{(E_2 - E_0)/[2(2+1)]} . \quad (8)$$

Note that $X_I = 1$ for a rigid rotor. The minimum rms deviation (i.e., for N_b and H_b) between experimental reduced γ energies and the corresponding result from Eq. (8) are called $\langle(\Delta X_b)^2\rangle^{1/2}$.

The moment of inertia $\mathscr{I}_I$ for any level I can be calculated from the $\mathscr{I}_0$ obtained as above and

$$\mathscr{I}_I/\mathscr{I}_0 = \zeta_I^N , \quad (9)$$

where ζ_I is the equilibrium value of y_I for level I in Eqs. (4) and (5) or (7a). The analysis of the present experimental results on Kr,[1] earlier results on Se from this laboratory,[16] and results on Ru and Mo[17,38,39] are given in Table VIII and Figs. 11 and 12. The sensitivity to N is given in Table IX for Kr. The circles in Fig. 2 are the results in Table VII.

Figure 11 shows that the best value of N in Eq. (6) varies rather smoothly and systematically with neutron number. It also shows that the VMI equation,[34] which is identical to Eqs. (6) and (7a) but with $N = 1$, is an approximation that obscures a systematic trend in the experimental results. Table IX shows that the rms discrepancy between experiment and Eqs. (6) and (7a) is approximately 2.5 times worse for $N = 1$ than for the best value N_b. Although it is recognized that the additional parameter N should improve the fit to experiment, it is also clear that in Fig. 11 the parameter N_b varies in a systematic way.

A nucleus like ^{78}Kr, which in Fig. 2 has a quasirotational level pattern (i.e., slowly increasing separation of yrast levels), has $N_b = 0.7$, a small hardness $H_b = 0.007$, and a small ground-state moment of inertia $\mathscr{I}_0 = 0.002$ keV^{-1}. A well-deformed nucleus like ^{172}Yb has $N_b = 3.4$, a very large hardness $H_b = 4100$, and a large ground-state moment of inertia $\mathscr{I}_0 = 0.038$ keV^{-1}.[37] Its $\mathscr{I}_{16} = 0.05$.

At another extreme is a nucleus such as ^{84}Kr in Fig. 2, whose yrast level separation reaches a maximum for $4^+ \to 2^+$. This nucleus requires a very large $N_b > 30$, a large hardness $H_b > 2300$, and has a small ground-state moment of inertia $\mathscr{I}_0 = 0.002$. Table VIII shows that the large H and large N in Eq. (7a) produce a maximum level separation for $4^+ \to 2^+$ and a monotonic decrease for larger I.

We see then that there are three classes of extreme conditions for energy in Eqs. (6) and (7a). One is $N \sim 1-4$ and $H \gg 1$, producing energies nearly $I(I+1)$. Another is $N \sim 1$ and $H \ll 1$, producing quasirotational sequences with adjacent level separations increasing more slowly with I and becoming almost constant at moderate I. The third is $N \gg 1$ and $H \gg 1$ producing a maximum level separation for small I and a monotonic decrease thereafter.

In spite of the gross difference in the patterns of yrast level energies for these three examples (^{78}Kr, ^{172}Yb, and ^{84}Kr), their moments of inertia (Table VIII) extrapolated to $I = 16$ are 0.023, 0.049, and 0.040, respectively.

TABLE IX. rms difference between experimental and theoretical normalized transition energies X_I for N_b, $N = 1.0$ and $N = 2.0$, respectively.

	$\langle(\Delta X_b)^2\rangle^{1/2}$ (%)	$\langle(\Delta X_1)^2\rangle^{1/2}$ (%)	$\langle(\Delta X_2)^2\rangle^{1/2}$ (%)
$^{84}_{36}$Kr	2.2	5.9	4.4
^{82}Kr	0.1	2.4	1.0
^{80}Kr	0.4	0.9	1.2
^{78}Kr	0.9	2.1	4.2

V. ISOMER IN ^{84}Kr

What is the origin of the long-lived transition feeding the 6^+ ground-state level in ^{84}Kr? The absence in Fig. 6 of any other transition of long-lived intensity comparable to that of the $6 \to 4$, $4 \to 2$, and $2 \to 0$ means that the isomeric transition must be of energy $\lesssim 100$ keV. If it were above 200 keV it would have to be of multipolarity $\gtrsim 4$ in order to be internally converted enough to mask the γ transition. The isomeric transition could not be from the 8^+ state in the ground-state band, since the $8 \to 6$ would have to be $\lesssim 100$ keV, as noted above, and the systematics exhibited in Table VIII are quite incompatible with such a low energy $8 \to 6$ in this band.

ACKNOWLEDGMENTS

We are indebted to Dr. G. L. Smith and Dr. R. A. Warner for helping to develop much of the experimental apparatus and many experimental techniques used during this work. The specific contributions by Dr. R. M. Lieder, E. Burns, and the crew and staff of the University of California at Davis, Crocker Nuclear Laboratory are greatly appreciated. We are also indebted to Dr. C. M. Lederer for providing his Mo and Ru data prior to publication.

---

†Much of this material is derived from a thesis submitted by D.G.M., in partial fulfillment of the requirements for a Ph.D. degree.

*Work supported in part by an U.S. Atomic Energy Commission sponsored Associated Western Universities, Inc. Graduate Fellowship. Present address: Michelson Laboratory, China Lake, California 93555.

‡Work supported in part by the U. S. Atomic Energy Commission.

[1]D. G. McCauley and J. E. Draper, Bull. Am. Phys. Soc. 15, 497 (1970).

[2]C. M. Huddelston and A. C. G. Mitchell, Phys. Rev. 88, 1350 (1952).

[3]G. M. Temmer and N. P. Heydenburg, Phys. Rev. 104, 967 (1956).

[4]N. P. Heydenburg, G. F. Pieper, and C. E. Anderson, Phys. Rev. 108, 106 (1957).

[5]S. L. Gupta and M. M. Bajaj, Australian J. Phys. 21, 649 (1968).

[6]E. Luikkonen, J. Hattula, and A. Antilla, Nucl. Phys. A138, 163 (1969).

[7]G. F. Meredith and R. A. Meyer, Nucl. Phys. A142, 513 (1970).

[8]G. Graeffe, S. Vaizala, and J. Heinonen, Nucl. Phys. A140, 161 (1970).

[9]C. M. Lederer, J. M. Hollander, and I. Perlman, *Table of Isotopes* (John Wiley & Sons, Inc., New York, 1967), 6th ed.

[10]E. Nolte, W. Kutschera, Y. Shida, and H. Morinaga, Phys. Letters 33B, 294 (1970).

[11]D. Ward, R. M. Diamond, and F. S. Stephens, Nucl. Phys. A117, 309 (1968).

[12]I. Bergstrom, C. J. Herrlander, A. Kerek, and A. Luukko, Nucl. Phys. A123, 99 (1969).

[13]G. L. Smith and J. E. Draper, Phys. Rev. C 1, 1548 (1970).

[14]R. A. Warner and J. E. Draper, Phys. Rev. C 1, 1069 (1970).

[15]E. Marshalek, L. Wu Person, and R. K. Sheline, Rev. Mod. Phys. 35, 108 (1963).

[16]R. M. Lieder and J. E. Draper, Phys. Rev. C 2, 531 (1970).

[17]C. M. Lederer, private communication.

[18]J. E. Draper and R. M. Lieder, Nucl. Phys. A141, 211 (1970).

[19]R. A. Warner, G. L. Smith, R. M. Lieder, and J. E. Draper, Nucl. Instr. Methods 75, 149 (1969).

[20]J. P. Welker and M. L. Perlman, Phys. Rev. 100, 74 (1955).

[21]N. R. Johnson and G. D. O'Kelley, Phys. Rev. 108, 82 (1957).

[22]G. A. Bartholomew, A. Doveika, K. M. Eastwook, S. Monaro, L. V. Broshev, A. M. Demidov, V. I. Pelekhov, L. L. Sokoloviskii, and I. V. Kurchatov, Nucl. Data A3, 367 (1967).

[23]*Nuclear Data Sheets*, compiled by K. Way *et al.* (Printing and Publishing Office, National Academy of Sciences–National Research Council, Washington, D. C.), Pt. 3.

[24]J. E. Sattizahn, J. D. Knight, and M. Kahn, J. Inorg. Nucl. Chem. 12, 206 (1960).

[25]T. A. Walkiewiez and E. Bleuler, Nucl. Phys. A136, 177 (1969).

[26]R. C. Etherton and W. H. Kelly, Nucl. Phys. 84, 129 (1966).

[27]N. E. Scott, J. W. Cobble, and P. J. Daly, Nucl. Phys. A119, 131 (1968).

[28]J. O. Newton, F. S. Stephens, R. M. Diamond, W. H. Kelly, and D. Ward, Nucl. Phys. A141, 631 (1970).

[29]L. S. Kisslinger and R. A. Sorensen, Rev. Mod. Phys. 35, 853 (1963).

[30]B. L. Birbrair, K. I. Erokhina, and I. K. Lemberg, Nucl. Phys. A145, 129 (1970).

[31]T. K. Das, R. M. Dreizler, and A. Klein, private communication.

[32]J. E. Draper, Phys. Letters 32B, 581 (1970).

[33]J.-P. Hazan and M. Blann, Phys. Rev. 137, B1202 (1965).

[34]M. A. J. Mariscotti, G. Scharff-Goldhaber, and B. Buck, Phys. Rev. 178, 1864 (1969).

[35]M. A. J. Mariscotti, Phys. Rev. Letters 24, 1242 (1970).

[36]G. Scharff-Goldhaber and A. S. Goldhaber, Phys. Rev. Letters 24, 1349 (1970).

[37]J. E. Draper, D. G. McCauley, and G. L. Smith, to be published.

[38]M. J. Jaklevic, C. M. Lederer, and J. M. Hollander, University of California Radiation Laboratory Report No. UCRL-18667, 1968 (unpublished).

[39]E. Cheifetz, R. C. Jared, S. G. Thompson, and J. B. Wilhelmy, University of California Radiation Laboratory Report No. UCRL-19584, 1970 (unpublished).